

Abdominal multi-organ segmentation in CT using Swinunter

Mingjin Chen¹, Yongkang He¹, and Yongyi Lu¹

¹ Guangdong University of Technology, Guangdong 51006, China

{2112103033}@mail2.gdut.edu.cn

Abstract. Abdominal multi-organ segmentation in computed tomography (CT) is crucial for many clinical applications including disease detection and treatment planning. Deep learning methods have shown unprecedented performance in this perspective. However, it is still quite challenging to accurately segment different organs utilizing a single network due to the vague boundaries of organs, the complex background, and the substantially different organ size scales. In this work we used make transformer-based model for training. It was found through previous years' competitions that basically all of the top 5 methods used CNN-based methods, which is likely due to the lack of data volume that prevents transformer-based methods from taking full advantage. The thousands of samples in this competition may enable the transformer-based model to have more excellent results. The results on the public validation set also show that the transformer-based model can achieve an acceptable result and inference time.

Keywords: Multi-organ segmentation · Deep learning · Another keyword.

1 Introduction

Automated medical image segmentation techniques [8] have shown prominence for providing an accurate and reproducible solution for organ segmentation. Recently, deep learning-based human organs segmentation techniques [17,11,18,10] have achieved state-of-the-art performance in various benchmarks [21,1]. These advances are mainly due to the powerful feature extraction capabilities of Convolutional Neural Networks (CNN)s. However, the limited kernel size of CNN-based techniques restricts their capability of learning long-range dependencies that are critical for accurate segmentation of tumors that appear in various shapes and sizes.

Although several efforts [3] have tried to address this limitation by increasing the receptive field of the convolutional kernels, the effective receptive field is still limited to local regions.

In order to extract more effective local and global contextual representations, Swin UNETR [5] have been proposed as a hierarchical vision transformer that

computes self-attention in an efficient shifted window partitioning scheme. Swin UNETR utilizes a U-shaped network with a Swin transformer as the encoder and connects it to a CNN-based decoder at different resolutions via skip connections.

In this report we used a transformer-based model for training. It was found through previous years' competitions that basically all of the top 5 methods used CNN-based methods, which is likely due to the lack of data volume that prevents transformer-based methods from taking full advantage. The thousands of samples in this competition may enable the transformer-based model to have more excellent results.

2 Method

2.1 Preprocessing

We first crop the non-zero regions of the image and resample the cropped data, and then we use Z-Score standardization to normalize the data. The Z-Score standardized formula is as follows:

$$z = \frac{x - \mu}{\sigma} \quad (1)$$

where μ is the average value of the CT value of the image label, and σ is the variance of the CT value of the image label.

2.2 Network

We use **Swin UNTER** [5] as our network for training and testing. It consists of a Transformer encoder and a CNN decoder. As shown in Fig.1, the input to the Swin UNETR model is a token with a patch resolution of (H, W, D) .

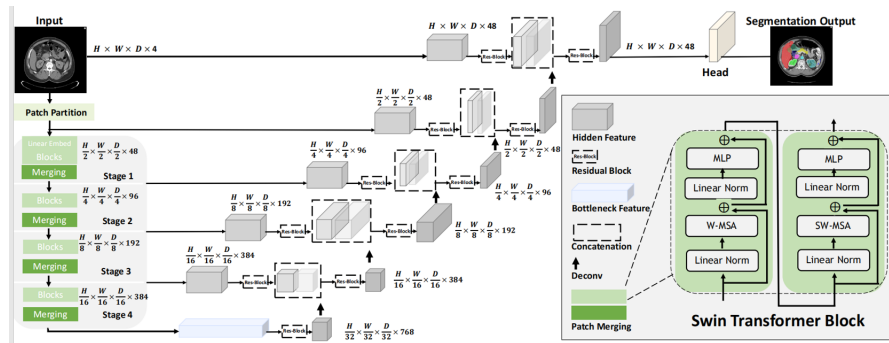


Fig. 1. Overview of the Swin UNETR architecture.

Encoder Swin UNTER has a U-shaped network design in which the extracted feature representations of the encoder are used in the decoder via skip connections at each resolution. The self-attention is computed into non-overlapping windows that are created in the partitioning stage for efficient token interaction modeling. It utilize windows of size $M \times M \times M$ to evenly partition a 3D token into $\lceil \frac{H'}{M} \rceil \times \lceil \frac{W'}{M} \rceil \times \lceil \frac{D'}{M} \rceil$ regions at a given layer l in the transformer encoder. Subsequently, in layer $l + 1$, the partitioned window regions are shifted by $\lceil \frac{M}{2} \rceil \times \lceil \frac{M}{2} \rceil \times \lceil \frac{M}{2} \rceil$ voxels. In subsequent layers, the regular and window partitioning multi-head self-attention (MSA) modules are used to learn effective local and global contextual representations.

Decoder At each stage i ($i \in 0, 1, 2, 3, 4$) in the encoder and the bottleneck ($i = 5$), the output feature representations are reshaped into size $\frac{H}{2^i} \times \frac{W}{2^i} \times \frac{D}{2^i}$ and fed into a residual block comprising of two $3 \times 3 \times 3$ convolutional layers that are normalized by instance normalization [22] layers. Subsequently, the resolution of the feature maps are increased by a factor of 2 using a deconvolutional layer and the outputs are concatenated with the outputs of the previous stage. The concatenated features are then fed into another residual block as previously described. The final segmentation outputs are computed by using a $1 \times 1 \times 1$ convolutional layer and a sigmoid activation function.

2.3 Loss function

we use the soft Dice loss functions, it has been proven to be robust in various medical image segmentation tasks [12]. It is computed in a voxel-wise manner as

$$L(G, Y) = 1 - \frac{2}{J} \sum_{j=1}^J \frac{\sum_{i=1}^I G_{i,j} Y_{i,j}}{\sum_{i=1}^I G_{i,j}^2 + \sum_{i=1}^I Y_{i,j}^2} \quad (2)$$

where I denotes voxels numbers; J is classes number; $Y_{i,j}$ and $G_{i,j}$ denote the probability of output and one-hot encoded ground truth for class j at voxel i , respectively.

2.4 Post-processing

In some computer vision tasks, it is necessary to do some post-processing on the output of the model to optimize the visual effect, and connected domain is a common post-processing method. Especially for segmentation tasks, sometimes there are some false positives in the output mask. Finding independent contours with small area through 3D connected domain and removing them can effectively improve the visual effect. We use connected domain principal component analysis to remove 3D small connected domains and retain the largest part of each label connected domain.

3 Experiments

3.1 Dataset and evaluation measures

The FLARE 2023 challenge is an extension of the FLARE 2021-2022 [14][15], aiming to aim to promote the development of foundation models in abdominal disease analysis. The segmentation targets cover 13 organs and various abdominal lesions. The training dataset is curated from more than 30 medical centers under the license permission, including TCIA [4], LiTS [2], MSD [20], KiTS [6,7], and AbdomenCT-1K [16]. The training set includes 4000 abdomen CT scans where 2200 CT scans with partial labels and 1800 CT scans without labels. The validation and testing sets include 100 and 400 CT scans, respectively, which cover various abdominal cancer types, such as liver cancer, kidney cancer, pancreas cancer, colon cancer, gastric cancer, and so on. The organ annotation process used ITK-SNAP [23], nnU-Net [9], and MedSAM [13].

The evaluation metrics encompass two accuracy measures—Dice Similarity Coefficient (DSC) and Normalized Surface Dice (NSD)—alongside two efficiency measures—running time and area under the GPU memory-time curve. These metrics collectively contribute to the ranking computation. Furthermore, the running time and GPU memory consumption are considered within tolerances of 15 seconds and 4 GB, respectively.

3.2 Implementation details

Environment settings The development environments and requirements are presented in Table 1.

Table 1. Development environments and requirements.

System	Ubuntu 18.04.5 LTS or Windows 11
CPU	AMD EPYC 7502 32-Core Processor
RAM	16×4GB; 2.67MT/s
GPU (number and type)	Four NVIDIA V100 16G
CUDA version	11.0
Programming language	Python 3.7.12
Deep learning framework	torch 1.12.0, torchvision 0.13.0
Specific dependencies	monai 0.9.0
Code	https://github.com/chanwendy/FLARE23

Training protocols The Training protocols are presented in Table 2. First, we use only partially labeled images to train a pretrain model, then we use this pretrain model to generate pseudo-labels for the unlabeled images as our labels, and then we use this pseudo-labeled as well as partially labeled data to continue to train the pretrain model to obtain our final model. For data enhancement we first convert all the images to the same spacing and then apply rotation, translation, and sampling of positive samples. For the training of the model we used AdamW as an optimizer with a weight decay of 0.05

Table 2. Training protocols.

Network initialization	"he" normal initialization
Batch size	2
Patch size	96×96×96
Total epochs	1000
Optimizer	AdamW
Initial learning rate (lr)	1e-4
Lr decay schedule	None
Training time	72.5 hours
Loss function	Dice
Number of model parameters	244.47M
Number of flops	59.32G
CO ₂ eq	1 Kg

4 Results and discussion

The average running time is 10s per case in inference phase. The maximum used GPU memory is 14129MB. Table 3 lists the results on the validation set. Overall, better results are achieved for larger and regular organs like the liver and the kidney. Worse results are achieved for smaller and complex organs like the gallbladder and the duodenum. These results indicate that it is difficult to handle the size variations utilizing the Swinunter, and specific modules should be designed to particularly address the issue.

4.1 Quantitative results on validation set

We use swinunter as our main network framework to first train our pretrain model with only partially labeled data, and then predict labels without labeled

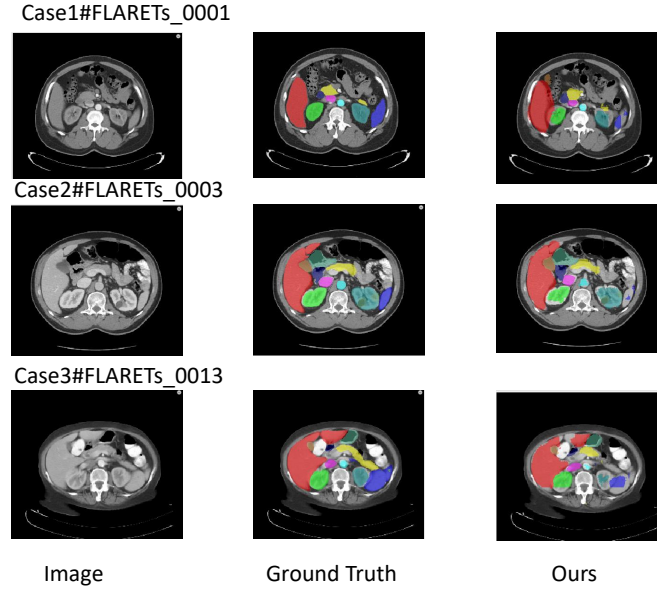


Fig. 2. Example segmentation results with high segmentation accuracy.

Table 3. The dice metrics of the prediction results of Swinunter on the open source validation set and The dice metrics of their embedding prediction results on the validation set.

Target	Public Validation		Online Validation		Testing	
	DSC(%)	NSD(%)	DSC(%)	NSD(%)	DSC(%)	NSD (%)
Liver	0.8969 ± 0.098	0.6019 ± 0.078	-	-		
Right Kidney	0.8800 ± 0.196	0.6045 ± 0.078	-	-		
Spleen	0.8741 ± 0.147	0.6013 ± 0.077	-	-		
Pancreas	0.8271 ± 0.091	0.6021 ± 0.077	-	-		
Aorta	0.877 ± 0.121	0.6049 ± 0.077	-	-		
Inferior vena cava	0.8620 ± 0.115	0.6077 ± 0.077	-	-		
Right adrenal gland	0.7252 ± 0.232	0.6079 ± 0.078	-	-		
Left adrenal gland	0.7192 ± 0.223	0.6075 ± 0.078	-	-		
Gallbladder	0.7954 ± 0.253	0.6078 ± 0.078	-	-		
Esophagus	0.7650 ± 0.167	0.6067 ± 0.078	-	-		
Stomach	0.9051 ± 0.072	0.6066 ± 0.078	-	-		
Duodenum	0.8360 ± 0.093	0.6074 ± 0.078	-	-		
Left kidney	0.8820 ± 0.157	0.6075 ± 0.078	-	-		
Tumor	0.7642 ± 0.186	0.6067 ± 0.078	-	-		
Average	0.8293 ± 0.061	0.6058 ± 0.002	-	-		

data as pseudo-labels by pretrain model. Finally the final model is obtained by fine-tuning the pretrain model with a mixture of pseudo-labeled data and partially labeled data. The final results on the publicly available 50 validation sets are shown in Table 3.

4.2 Qualitative results on validation set

Fig. 2 presents the segmentation results of three cases for which satisfactory segmentation accuracy is achieved. Fig. 3 shows the segmentation results of three cases for which low segmentation accuracy is achieved. It can be observed that for those easy samples, the background is quite simple, whereas for hard samples, the background is quite complex. Meanwhile, the most obvious problem for the low accuracy is the under-segmentation of the small organs and the over-segmentation of the big organs. Possible reasons could be that the model training is not sufficient or that the model complexity is not enough due to the small training data we utilized. I believe more accurate results can be obtained if we exploit the unlabeled data in an effective way.

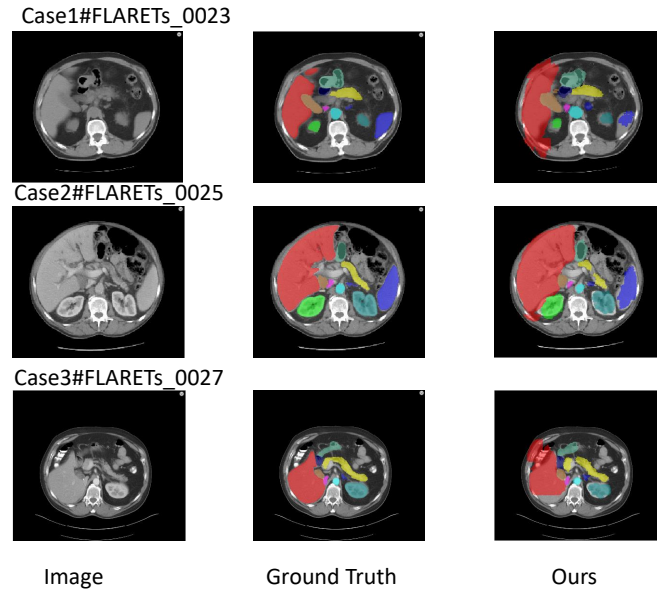


Fig. 3. Example segmentation results with low segmentation accuracy.

4.3 Limitation and future work

Although we have thousands of training samples, the fact that the labels are partially labeled and half of the data is pseudo-labeled leads to unstable training when fine-tuning the pretrain model, which can easily cause the model to overfit into one of the organs.

In future work, we will make a partial decoder for partially labeled data to decode a specific organ, and for the problem of pseudo-labeling accuracy, we will consider some newer methods to update the pseudo-labeling accuracy to get a better fine-tuned model.

5 Conclusion

We used a transformer-based model as our main framework because the amount of data for this competition was large enough, compared to last year, so we thought that a large amount of data might be more suitable for a transformer-based model. The results of our model have an acceptable effect on the open source validation set as well as the speed of inference. Since our current work does not require excessive accuracy of pseudo-labeling, which is our drawback, we need to further consider the accuracy of pseudo-labeling and the correct decoding of some of the labels in our future work.

Acknowledgements The authors of this paper declare that the segmentation method they implemented for participation in the FLARE 2023 challenge has not used any pre-trained models nor additional datasets other than those provided by the organizers. The proposed solution is fully automatic without any manual intervention. We thank all the data owners for making the CT scans publicly available and CodaLab [19] for hosting the challenge platform.

References

1. Bakas, S., Reyes, M., Jakab, A., Bauer, S., Rempfler, M., Crimi, A., Shinohara, R.T., Berger, C., Ha, S.M., Rozycki, M., et al.: Identifying the best machine learning algorithms for brain tumor segmentation, progression assessment, and overall survival prediction in the brats challenge. arXiv preprint arXiv:1811.02629 (2018)
2. Bilic, P., Christ, P., Li, H.B., Vorontsov, E., Ben-Cohen, A., Kaissis, G., Szeskin, A., Jacobs, C., Mamani, G.E.H., Chartrand, G., Lohöfer, F., Holch, J.W., Sommer, W., Hofmann, F., Hostettler, A., Lev-Cohain, N., Drozdal, M., Amitai, M.M., Vivanti, R., Sosna, J., Ezhov, I., Sekuboyina, A., Navarro, F., Kofler, F., Paetzold, J.C., Shit, S., Hu, X., Lipková, J., Rempfler, M., Piraud, M., Kirschke, J., Wiestler, B., Zhang, Z., Hülsemeyer, C., Beetz, M., Ettliger, F., Antonelli, M., Bae, W., Bellver, M., Bi, L., Chen, H., Chlebus, G., Dam, E.B., Dou, Q., Fu, C.W., Georgescu, B., i Nieto, X.G., Gruen, F., Han, X., Heng, P.A., Hesser, J., Moltz, J.H., Igel, C., Isensee, F., Jäger, P., Jia, F., Kaluva, K.C., Khened, M., Kim, I., Kim, J.H., Kim, S., Kohl, S., Konopczynski, T., Kori, A., Krishnamurthi, G., Li, F., Li, H., Li, J.,

- Li, X., Lowengrub, J., Ma, J., Maier-Hein, K., Maninis, K.K., Meine, H., Merhof, D., Pai, A., Perslev, M., Petersen, J., Pont-Tuset, J., Qi, J., Qi, X., Rippel, O., Roth, K., Sarasua, I., Schenk, A., Shen, Z., Torres, J., Wachinger, C., Wang, C., Weninger, L., Wu, J., Xu, D., Yang, X., Yu, S.C.H., Yuan, Y., Yue, M., Zhang, L., Cardoso, J., Bakas, S., Braren, R., Heinemann, V., Pal, C., Tang, A., Kadoury, S., Soler, L., van Ginneken, B., Greenspan, H., Joskowicz, L., Menze, B.: The liver tumor segmentation benchmark (lits). *Medical Image Analysis* **84**, 102680 (2023) [4](#)
3. Chen, C., Liu, X., Ding, M., Zheng, J., Li, J.: 3d dilated multi-fiber network for real-time brain tumor segmentation in mri. In: *Medical Image Computing and Computer Assisted Intervention–MICCAI 2019: 22nd International Conference, Shenzhen, China, October 13–17, 2019, Proceedings, Part III* **22**. pp. 184–192. Springer (2019) [1](#)
 4. Clark, K., Vendt, B., Smith, K., Freymann, J., Kirby, J., Koppel, P., Moore, S., Phillips, S., Maffitt, D., Pringle, M., Tarbox, L., Prior, F.: The cancer imaging archive (tcia): maintaining and operating a public information repository. *Journal of Digital Imaging* **26**(6), 1045–1057 (2013) [4](#)
 5. Hatamizadeh, A., Nath, V., Tang, Y., Yang, D., Roth, H.R., Xu, D.: Swin unetr: Swin transformers for semantic segmentation of brain tumors in mri images. In: *International MICCAI Brainlesion Workshop*. pp. 272–284. Springer (2021) [1](#), [2](#)
 6. Heller, N., Isensee, F., Maier-Hein, K.H., Hou, X., Xie, C., Li, F., Nan, Y., Mu, G., Lin, Z., Han, M., Yao, G., Gao, Y., Zhang, Y., Wang, Y., Hou, F., Yang, J., Xiong, G., Tian, J., Zhong, C., Ma, J., Rickman, J., Dean, J., Stai, B., Tejpaul, R., Oestreich, M., Blake, P., Kaluzniak, H., Raza, S., Rosenberg, J., Moore, K., Walczak, E., Rengel, Z., Edgerton, Z., Vasdev, R., Peterson, M., McSweeney, S., Peterson, S., Kalapara, A., Sathianathen, N., Papanikolopoulos, N., Weight, C.: The state of the art in kidney and kidney tumor segmentation in contrast-enhanced ct imaging: Results of the kits19 challenge. *Medical Image Analysis* **67**, 101821 (2021) [4](#)
 7. Heller, N., McSweeney, S., Peterson, M.T., Peterson, S., Rickman, J., Stai, B., Tejpaul, R., Oestreich, M., Blake, P., Rosenberg, J., et al.: An international challenge to use artificial intelligence to define the state-of-the-art in kidney and kidney tumor segmentation in ct imaging. *American Society of Clinical Oncology* **38**(6), 626–626 (2020) [4](#)
 8. Huo, Y., Xu, Z., Xiong, Y., Aboud, K., Parvathaneni, P., Bao, S., Bermudez, C., Resnick, S.M., Cutting, L.E., Landman, B.A.: 3d whole brain segmentation using spatially localized atlas network tiles. *NeuroImage* **194**, 105–119 (2019) [1](#)
 9. Isensee, F., Jaeger, P.F., Kohl, S.A., Petersen, J., Maier-Hein, K.H.: nnu-net: a self-configuring method for deep learning-based biomedical image segmentation. *Nature Methods* **18**(2), 203–211 (2021) [4](#)
 10. Isensee, F., Jäger, P.F., Full, P.M., Vollmuth, P., Maier-Hein, K.H.: nnu-net for brain tumor segmentation. In: *Brainlesion: Glioma, Multiple Sclerosis, Stroke and Traumatic Brain Injuries: 6th International Workshop, BrainLes 2020, Held in Conjunction with MICCAI 2020, Lima, Peru, October 4, 2020, Revised Selected Papers, Part II* **6**. pp. 118–132. Springer (2021) [1](#)
 11. Jiang, Z., Ding, C., Liu, M., Tao, D.: Two-stage cascaded u-net: 1st place solution to brats challenge 2019 segmentation task. In: *Brainlesion: Glioma, Multiple Sclerosis, Stroke and Traumatic Brain Injuries: 5th International Workshop, BrainLes 2019, Held in Conjunction with MICCAI 2019, Shenzhen, China, October 17, 2019, Revised Selected Papers, Part I* **5**. pp. 231–241. Springer (2020) [1](#)

12. Ma, J., Chen, J., Ng, M., Huang, R., Li, Y., Li, C., Yang, X., Martel, A.L.: Loss odyssey in medical image segmentation. *Medical Image Analysis* **71**, 102035 (2021) [3](#)
13. Ma, J., Wang, B.: Segment anything in medical images. arXiv preprint arXiv:2304.12306 (2023) [4](#)
14. Ma, J., Zhang, Y., Gu, S., An, X., Wang, Z., Ge, C., Wang, C., Zhang, F., Wang, Y., Xu, Y., Gou, S., Thaler, F., Payer, C., Štern, D., Henderson, E.G., McSweeney, D.M., Green, A., Jackson, P., McIntosh, L., Nguyen, Q.C., Qayyum, A., Conze, P.H., Huang, Z., Zhou, Z., Fan, D.P., Xiong, H., Dong, G., Zhu, Q., He, J., Yang, X.: Fast and low-gpu-memory abdomen ct organ segmentation: The flare challenge. *Medical Image Analysis* **82**, 102616 (2022) [4](#)
15. Ma, J., Zhang, Y., Gu, S., Ge, C., Ma, S., Young, A., Zhu, C., Meng, K., Yang, X., Huang, Z., Zhang, F., Liu, W., Pan, Y., Huang, S., Wang, J., Sun, M., Xu, W., Jia, D., Choi, J.W., Alves, N., de Wilde, B., Koehler, G., Wu, Y., Wiesenfarth, M., Zhu, Q., Dong, G., He, J., the FLARE Challenge Consortium, Wang, B.: Unleashing the strengths of unlabeled data in pan-cancer abdominal organ quantification: the flare22 challenge. arXiv preprint arXiv:2308.05862 (2023) [4](#)
16. Ma, J., Zhang, Y., Gu, S., Zhu, C., Ge, C., Zhang, Y., An, X., Wang, C., Wang, Q., Liu, X., Cao, S., Zhang, Q., Liu, S., Wang, Y., Li, Y., He, J., Yang, X.: Abdomenct-1k: Is abdominal organ segmentation a solved problem? *IEEE Transactions on Pattern Analysis and Machine Intelligence* **44**(10), 6695–6714 (2022) [4](#)
17. Myronenko, A.: 3d mri brain tumor segmentation using autoencoder regularization. In: *Brainlesion: Glioma, Multiple Sclerosis, Stroke and Traumatic Brain Injuries: 4th International Workshop, BrainLes 2018, Held in Conjunction with MICCAI 2018, Granada, Spain, September 16, 2018, Revised Selected Papers, Part II* 4. pp. 311–320. Springer (2019) [1](#)
18. Myronenko, A., Hatamizadeh, A.: Robust semantic segmentation of brain tumor regions from 3d mris. In: *Brainlesion: Glioma, Multiple Sclerosis, Stroke and Traumatic Brain Injuries: 5th International Workshop, BrainLes 2019, Held in Conjunction with MICCAI 2019, Shenzhen, China, October 17, 2019, Revised Selected Papers, Part II* 5. pp. 82–89. Springer (2020) [1](#)
19. Pavao, A., Guyon, I., Letournel, A.C., Tran, D.T., Baro, X., Escalante, H.J., Escalera, S., Thomas, T., Xu, Z.: Codalab competitions: An open source platform to organize scientific challenges. *Journal of Machine Learning Research* **24**(198), 1–6 (2023) [8](#)
20. Simpson, A.L., Antonelli, M., Bakas, S., Bilello, M., Farahani, K., van Ginneken, B., Kopp-Schneider, A., Landman, B.A., Litjens, G., Menze, B., Ronneberger, O., Summers, R.M., Bilic, P., Christ, P.F., Do, R.K.G., Gollub, M., Golia-Pernicka, J., Heckers, S.H., Jarnagin, W.R., McHugo, M.K., Napel, S., Vorontsov, E., Maier-Hein, L., Cardoso, M.J.: A large annotated medical image dataset for the development and evaluation of segmentation algorithms. arXiv preprint arXiv:1902.09063 (2019) [4](#)
21. Simpson, A.L., Antonelli, M., Bakas, S., Bilello, M., Farahani, K., Van Ginneken, B., Kopp-Schneider, A., Landman, B.A., Litjens, G., Menze, B., et al.: A large annotated medical image dataset for the development and evaluation of segmentation algorithms. arXiv preprint arXiv:1902.09063 (2019) [1](#)
22. Ulyanov, D., Vedaldi, A., Lempitsky, V.: Instance normalization: The missing ingredient for fast stylization. arXiv preprint arXiv:1607.08022 (2016) [3](#)
23. Yushkevich, P.A., Gao, Y., Gerig, G.: Itk-snap: An interactive tool for semi-automatic segmentation of multi-modality biomedical images. In: *Annual Inter-*

national Conference of the IEEE Engineering in Medicine and Biology Society. pp. 3342–3345 (2016) [4](#)

Table 4. Checklist Table. Please fill out this checklist table in the answer column.

Requirements	Answer
A meaningful title	Yes/No
The number of authors (≤ 6)	Number
Author affiliations, Email, and ORCID	Yes/No
Corresponding author is marked	Yes/No
Validation scores are presented in the abstract	Yes/No
Introduction includes at least three parts: background, related work, and motivation	Yes/No
A pipeline/network figure is provided	Figure number
Pre-processing	Page number
Strategies to use the partial label	Page number
Strategies to use the unlabeled images.	Page number
Strategies to improve model inference	Page number
Post-processing	Page number
Dataset and evaluation metric section is presented	Page number
Environment setting table is provided	Table number
Training protocol table is provided	Table number
Ablation study	Page number
Visualized segmentaiton example is provided	Figure number
Limitation and future work are presented	Yes/No
Reference format is consistent.	Yes/No